Neutron powder diffraction study (T = 4.2-300 K) and polarization analysis of $YBaCuFeO_{5+\delta}$

1998 J. Phys.: Condens. Matter 10 1247

(http://iopscience.iop.org/0953-8984/10/6/008)

J. Phys.: Condens. Matter **10** (1998) 1247–1258. Printed in the UK PII: S0953-8984(98)80651-6

Neutron powder diffraction study ($T = 4.2$–300 K) and polarization analysis of $YBaCuFeO_{5+\delta}$

A W Mombrú†‡, K Prassides‡, C Christides‡§, R Erwin‖, M Pissas§, C Mitros§ and D Niarchos§

† Laboratorio de Cristalografía, Cátedra de Física, Facultad de Química, PO Box 1157, CP 11800, Montevideo, Uruguay

‡ School of Chemistry, Physics and Environmental Science, University of Sussex, Brighton BN1 9QJ, UK

§ Institute of Materials Science, NCSR 'Demokritos', 153 10 Aghia Paraskevi, Attiki, Greece

‖ Reactor Radiation Division, National Institute of Standards and Technology, Gaithersburg, MD 20899, USA

Received 6 January 1997, in final form 14 November 1997

Abstract. The crystal and magnetic structures of the perovskite $YBaCuFeO_{5+\delta}$ have been studied in the temperature range $T = 4.2$–300 K by powder neutron diffraction. In addition to the antiferromagnetic ordering transition at $T_N = 442$ K, a commensurate–incommensurate magnetic transition is detected at $T'_N = 190$ K. Below this temperature, two sets of satellite peaks surround the $(1/2, 1/2, 1/2)$ magnetic peak at $d \sim 5.15$ Å, collapsing into a single set of satellites below 155 K. Polarization analysis has been performed to confirm the magnetic nature of the $(1/2, 1/2, 1/2)^{\pm}$ satellites.

1. Introduction

The oxygen deficient perovskite $YBaCuFeO_{5+\delta}$ was first observed [1] as an impurity in Fe-doped samples of the superconductor $YBa_2Cu_3O_{7-\delta}$ and of the 'green phase' Y_2BaCuO_5. It belongs to the $YBaFe_{2-x}Cu_xO_{5.5-x/2+\delta}$ series with $x = 1$ and adopts a tetragonal structure with cell parameters $a = b = 3.867$ Å, $c = 7.656$ Å ($\sim 2a$). It was found to consist of $[CuFeO_{10}]_\infty$ bilayers of corner-sharing CuO_5 and FeO_5 square pyramids (figure 1), thus providing an example of the rare five-fold square-pyramidal coordination of Fe^{3+}. Y^{3+} layers (coordination number 8) separate the $(CuFeO_{10})$ bilayers and accommodate the oxygen vacancies, while the Ba^{2+} ions (coordination number 12) are located within the bilayer spacing, in a way reminiscent of that in the $YBa_2Cu_3O_{7-\delta}$ structure. Indeed, the structure can be derived from that of $YBa_2Cu_3O_{7-\delta}$ by removing the Cu(1)O layers and half of the apical oxygen atoms, so that the pyramids between two yttrium layers share apical oxygens. However, the elongated pyramids situated on each side of an yttrium layer are not exactly identical. The crystal structure was determined by neutron powder diffraction to be tetragonal (space group $P4mm$) with the Fe^{3+} and Cu^{2+} ions distributed over two symmetry-inequivalent crystal sites [1].

More recent ^{57}Fe Mössbauer [2, 3] results revealed an antiferromagnetic ordering transition at $T_N = 446$ K, but were only consistent with the existence of a single unique Fe^{3+} site; this implied that the Fe^{3+} and Cu^{2+} ions were fully ordered, each occupying a single site in the $P4mm$ unit cell. A recent Raman and infrared spectroscopic study

0953-8984/98/061247+12$19.50

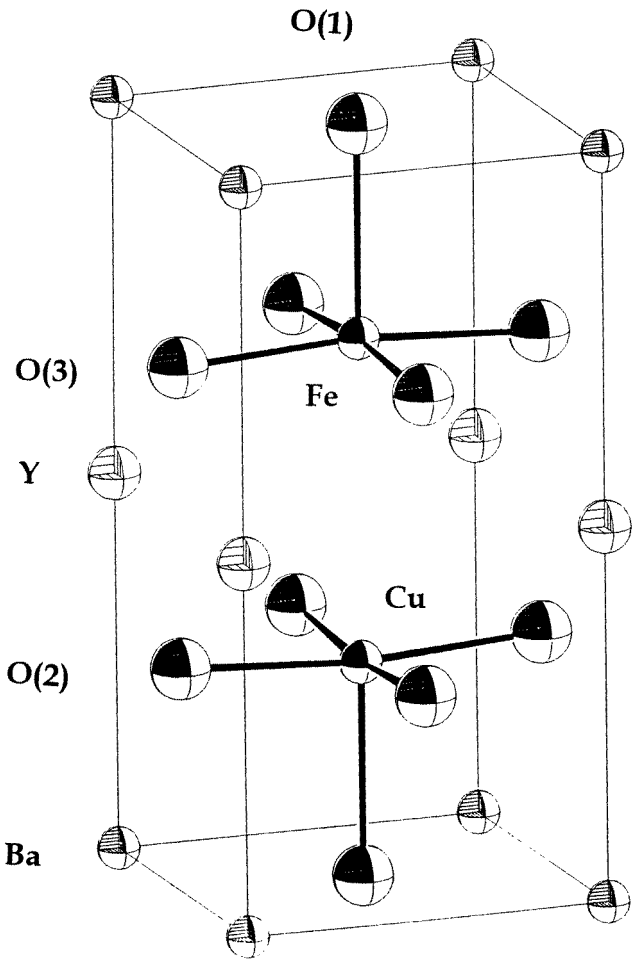

Figure 1. Crystal structure of $YBaCuFeO_5$.

[4] similarly necessitated the adoption of an acentric space group. The crystal structure of $YBaCuFeO_5$ has been also determined by single-crystal x-ray diffraction [5]. The magnetic structure has been studied by powder neutron diffraction [6, 7] and a transition to an incommensurate magnetic structure was identified below ∼230 K. This paper reports further powder diffraction work on $YBaCuFeO_{5+\delta}$ using both unpolarized and polarized neutrons.

2. Experimental details

2.1. Sample preparation

The $YBaCuFeO_{5+\delta}$ sample was prepared in air by standard solid-state reactions as follows: stoichiometric amounts of Y_2O_3, $BaCO_3$, CuO and Fe_2O_3 were fired at 900 °C for 12 h; the mixture was then ground and heated at 1000 °C for an additional 12 h. Phase purity was established by recording x-ray powder diffraction profiles at room temperature with a

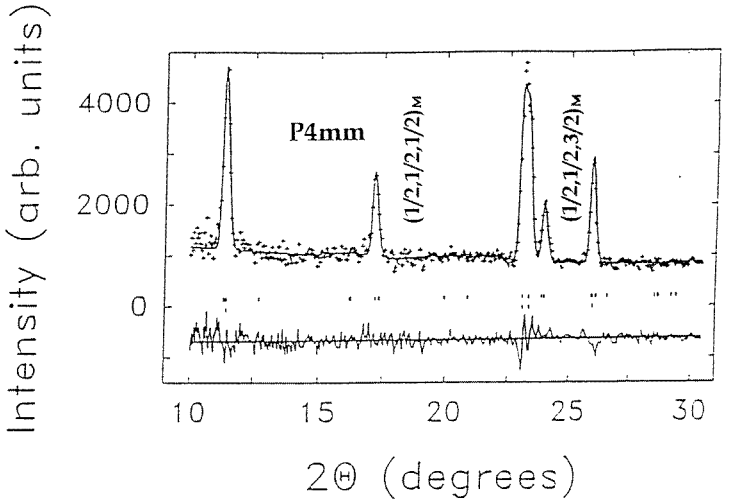

(a)

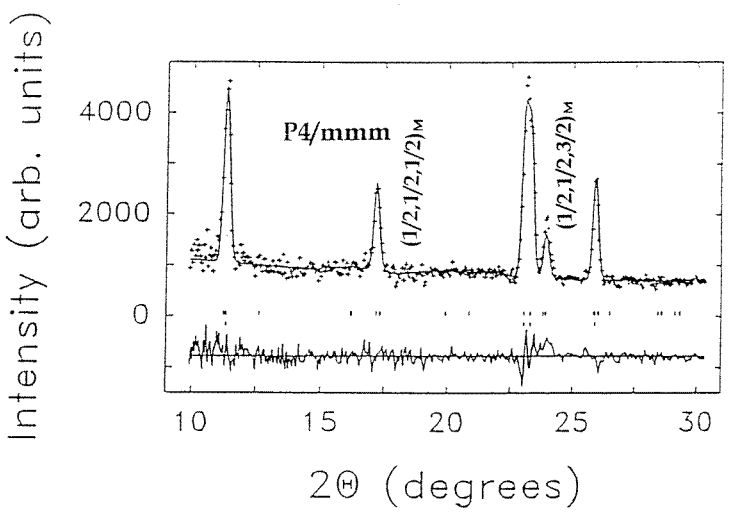

(b)

Figure 2. Neutron diffraction profile of $YBaCuFeO_{5+\delta}$ at room temperature and the results of the Rietveld refinements in the 2θ range 10°–30°: (a) space group $P4mm$ and (b) space group $P4/mmm$. Upper tick marks show the positions for magnetic peaks and lower tick marks the positions for nuclear peaks.

Siemens D5000 diffractometer. Thermogravimetric analysis using a Perkin–Elmer TGS-2 apparatus, was employed to determine the excess oxygen present as $\delta = 0.08$.

2.2. Data collection

A powder neutron diffraction dataset was collected at room temperature with the high-resolution BT1 diffractometer at the National Institute of Standards and Technology, Gaithersburg, MD, USA, using neutrons with a mean wavelength of 1.539 Å. Data were

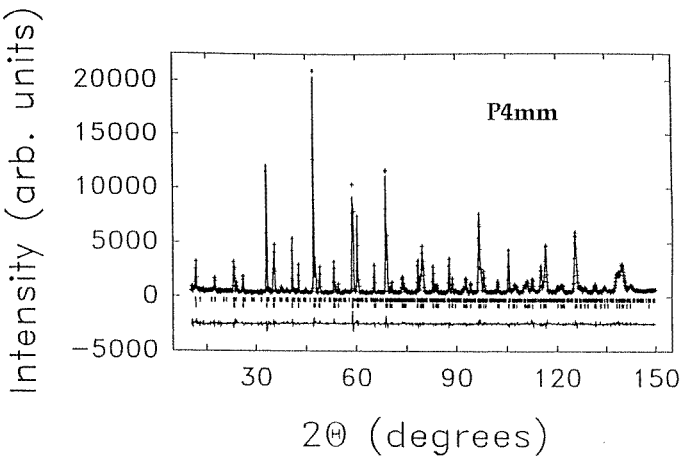

Figure 3. Neutron diffraction profile of $YBaCuFeO_{5+\delta}$ at room temperature and Rietveld refinement in the 2θ range 10°–150° (space group $P4mm$). Upper tick marks show the positions for magnetic peaks and lower tick marks the positions for nuclear peaks.

recorded for a 2θ range of 10–150° in steps of 0.05°. Low-temperature diffraction data in the 2.1–7.8 Å d-spacing range were collected between 4.2 and 200 K using the backscattering detectors of the IRIS instrument at the ISIS spallation neutron source, Rutherford Appleton Laboratory, UK.

Polarized neutron scattering measurements at 10 K were performed with the polarized beam BT2 spectrometer at NIST, Gaithersburg, MD, USA, using a $20' - 20' - 40' - 40'$ collimation. The incident beam was monochromated and polarized by a vertically magnetized focusing Heusler (111) alloy, and the polarization of the scattered neutrons was analysed by a supermirror. A PG filter was employed to suppress higher-order wavelengths, and vertical guide fields were employed along the neutron path to prevent depolarization of the beam. The measurements (incident neutron energy, $E_i = 14.8$ meV) were carried out under horizontal and vertical fields in the Q-ranges 1.08–1.32 Å^{-1} (region of the $(1/2, 1/2, 1/2)$ magnetic peak) and 2.25–2.40 Å^{-1} (region of the (102) and (110) nuclear peaks).

3. Nuclear and magnetic structure at room temperature

Rietveld analysis of the neutron diffraction profile at room temperature was performed using the GSAS programme suite [8]. In view of the earlier structural work on the subject [1, 3, 5–7], three structural models were considered: (a) completely disordered structure with the Fe^{3+} and Cu^{2+} ions statistically distributed in the Fe/Cu–O_2 layers ($P4/mmm$ space group); (b) fully ordered structure in which the Fe^{3+} and Cu^{2+} ions occupy distinct crystallographic sites ($P4mm$ space group) and (c) partially disordered structure in which partial occupation of the Fe^{3+} (or Cu^{2+}) site by Cu^{2+} (or Fe^{3+}) was allowed ($P4mm$ space group). Model (c) was immediately discarded as refinement of the occupancy factors of Fe^{3+} and Cu^{2+} rapidly led to the ordered model (b).

Satisfactory refinements of the nuclear structure were obtained for both models (a) and (b). The agreement factors obtained in the two refinements are as follows: $R_{wp} = 6.90\%$, $\chi^2 = 0.64$ for space group $P4mm$ and $R_{wp} = 7.04\%$, $\chi^2 = 0.67$ for space group $P4/mmm$.

However, using Hamilton's criterion [9], the improvement in the refinement on going from model (a) to (b) is not statistically significant, and we cannot reject the $P4/mmm$ structure on the basis of the nuclear profile refinements. We also note that for both sets of refinements, no excess oxygen concentration in the vacant pseudo-octahedral position was apparent with the excess oxygen fraction refining to 0.02(2).

Table 1. Final structural and magnetic parameters derived from the Rietveld refinements of $YBaCuFeO_{5+\delta}$ at room temperature (nuclear space groups $P4mm$ and $P4/mmm$, magnetic propagation vector $\boldsymbol{k} = (1/2, 1/2, 1/2)$).

Atom	Site	x/a	y/b	z/c	$U(\times 100)$ (Å^2)	$\mu_\perp$ (μ_B)	$\mu_\parallel$ (μ_B)
$P4mm$							
Y	1a	0	0	0.46992	$U_{11} = 0.52(4)$		
					$U_{33} = 1.0(1)$		
Ba	1a	0	0	−0.030(3)	$U_{11} = 0.36(7)$		
					$U_{33} = 3.2(2)$		
Fe	1b	1/2	1/2	0.700(1)	$U_{11} = 0.3(1)$	2.33(9)	0.7(2)
					$U_{33} = 3.1(3)$		
Cu	1b	1/2	1/2	0.235(1)	$U = 0.4(1)$	0.47(8)	0.4(1)
O(1)	1b	1/2	1/2	−0.045(1)	$U = 1.04(7)$		
O(2)	2c	1/2	0	0.280(1)	$U = 0.8(1)$		
O(3)	2c	1/2	0	0.649(1)	$U_{11} = 0.3(1)$		
					$U_{22} = 0.2(1)$		
					$U_{33} = 1.5(2)$		
Lattice constants: $a = 3.869\,66(6)$ Å, $c = 7.6613(2)$ Å							
R-factors: $R_{wp} = 6.90\%$, $R_p = 5.73\%$, $\chi^2 = 0.63$, $R_{mag} = 22.6\%$ (2θ range 10°–68°)							
$P4/mmm$							
Y	1b	0	0	0.5	$U = 0.68(3)$		
Ba	1a	0	0	0	$U_{11} = 0.52(6)$		
					$U_{33} = 2.9(2)$		
Fe	2h	1/2	1/2	0.2530(4)	$U = 0.16(9)$	2.54(9)	0.9(2)
Cu	2h	1/2	1/2	0.2833(4)	$U = 0.70(8)$	0.37(8)	0.4(1)
O(1)	1c	1/2	1/2	0	$U_{11} = 0.96(7)$		
					$U_{33} = 2.3(1)$		
O(2)	4i	1/2	0	0.3160(1)	$U_{11} = 0.64(4)$		
					$U_{22} = 0.48(4)$		
					$U_{33} = 1.27(5)$		
Lattice constants: $a = 3.869\,63(7)$ Å, $c = 7.6612(2)$ Å							
R-factors: $R_{wp} = 7.09\%$, $R_p = 5.89\%$, $\chi^2 = 0.67$, $R_{mag} = 27.6\%$ (2θ range 10°–68°)							

The determination of the magnetic structure for the two possible structural models was aided by the fact that all the magnetic origin peaks indexed on the basis of the chemical unit cell as $(h/2, k/2, l/2)$ with h, k, l = odd; this implied an enlarged magnetic unit cell with $a_M = 2a$ and $c_M = 2c$ and is only consistent with magnetic ordering schemes of both the CuO_2 and FeO_2 layers along the c-axis of the form $+[+-]-$ and $+[--]+$ (using the labelling scheme introduced earlier in [7] with the bracket corresponding to the position of the yttrium).

For the $P4mm$ structure, Rietveld profile refinements established the best model as $(+[--]+)_{x,y}$ and $(+[+-]-)_z$. In this ordered model, the μ_x- and μ_y-components of oxygen-sharing Fe^{3+} and Cu^{2+} ions point to the same direction, while the μ_z-components

Table 2. Selected bond distances (Å) and angles (°) in $YBaCuFeO_{5+\delta}$ at room temperature.

Space group	$P4mm$	$P4/mmm$
Cu–O_{eq}	1.967(2)	1.9509(4)
Cu–O_{ax}	2.142(9)	2.171(3)
Fe–O_{eq}	1.975(2)	1.9941(7)
Fe–O_{ax}	1.954(8)	1.938(3)
O_{eq}–Cu–O_{eq}	88.2(1)	89.06(2)
O_{eq}–Cu–O_{ax}	100.3(3)	97.3(1)
O_{eq}–Fe–O_{eq}	87.7(1)	86.64(4)
O_{eq}–Fe–O_{ax}	101.5(3)	104.00(8)

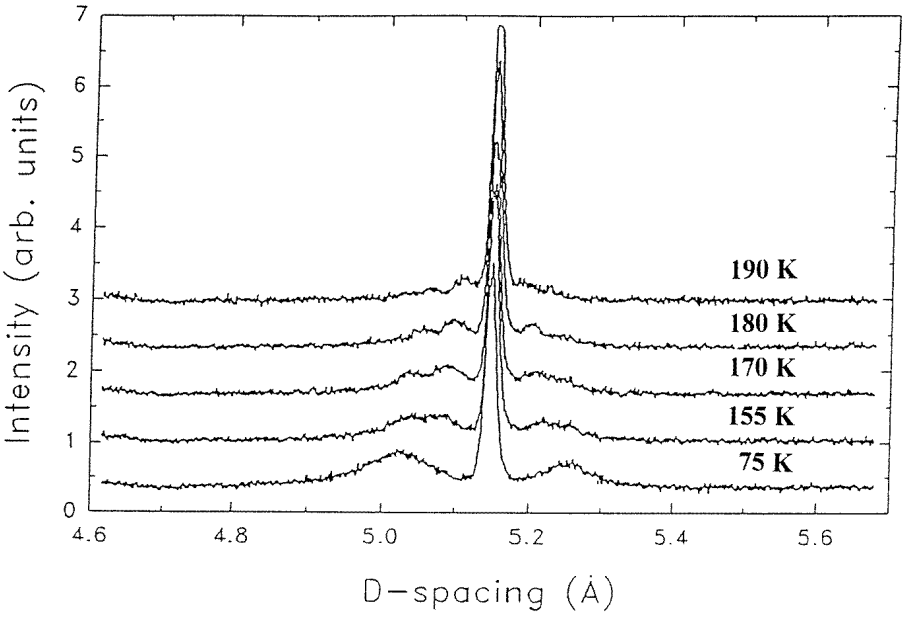

Figure 4. Temperature evolution of the neutron diffraction profile of $YBaCuFeO_{5+\delta}$ in the vicinity of the $(1/2, 1/2, 1/2)$ magnetic peak ($T = 75$, 155, 170, 180 and 190 K).

are antiparallel. The resulting magnetic moments associated with the Fe^{3+} and Cu^{2+} sublattices are $\mu_{Fe} = 2.43(5)\mu_B$ and $\mu_{Cu} = 0.6(1)\mu_B$, respectively, in agreement with earlier reports [6, 7]. The iron and copper magnetic moments are found to form angles of 73(5)° and 50(15)° with the c-axis, respectively. The reliability factors for this model were $R_{wp} = 6.90\%$, $\chi^2 = 0.63$.

For the fully disordered $P4/mmm$ structure, an identical $(+[--]+)_{x,y}$ and $(+[+-]-)_z$ ordering sequence was found to be in best agreement with the data. Again oxygen-sharing (Fe^{3+}/Cu^{2+}) ions exhibit magnetic moments with parallel x- and y-components and antiparallel z-component. The derived magnetic moments are now $\mu_{Fe} = 2.69(5)\mu_B$ and $\mu_{Cu} = 0.5(1)\mu_B$, the angles they form with the c-axis 70(5)° and 44(15)° for Fe^{3+} and Cu^{2+} ions, respectively, and the reliability factors of the Rietveld refinement $R_{wp} = 7.09\%$, $\chi^2 = 0.67$.

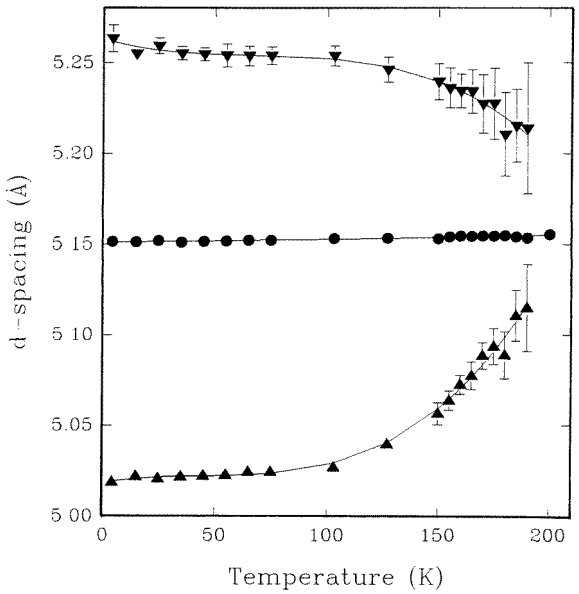

Figure 5. Evolution of the position of the $(1/2, 1/2, 1/2)^{\pm}$ magnetic satellites (triangles) with temperature. The full circles (●) show the position of the $(1/2, 1/2, 1/2)$ magnetic peak.

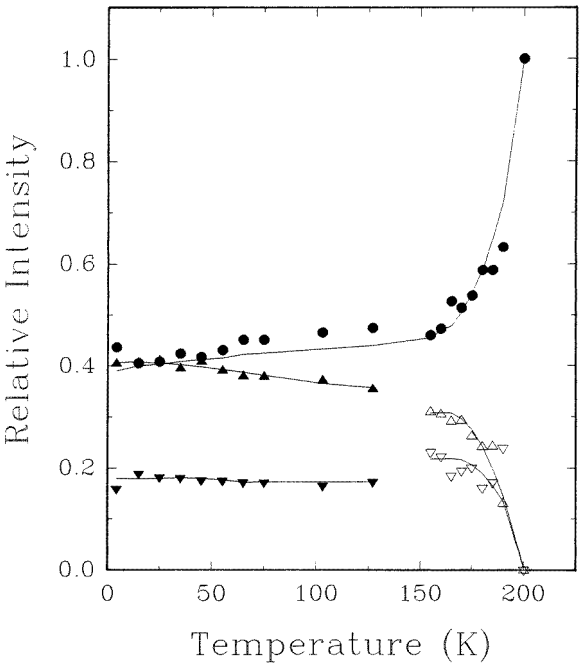

Figure 6. Evolution of the relative intensities of the $(1/2, 1/2, 1/2)$ magnetic peak (●) and its satellites (triangles) normalized to the total intensity with temperature.

Focusing now on the magnetic reliability factors, R_{mag}, we find values of 22.6% and 27.6% for the $P4mm$ and $P4/mmm$ models, respectively (2θ range $= 10^{\circ}$–68°). It is

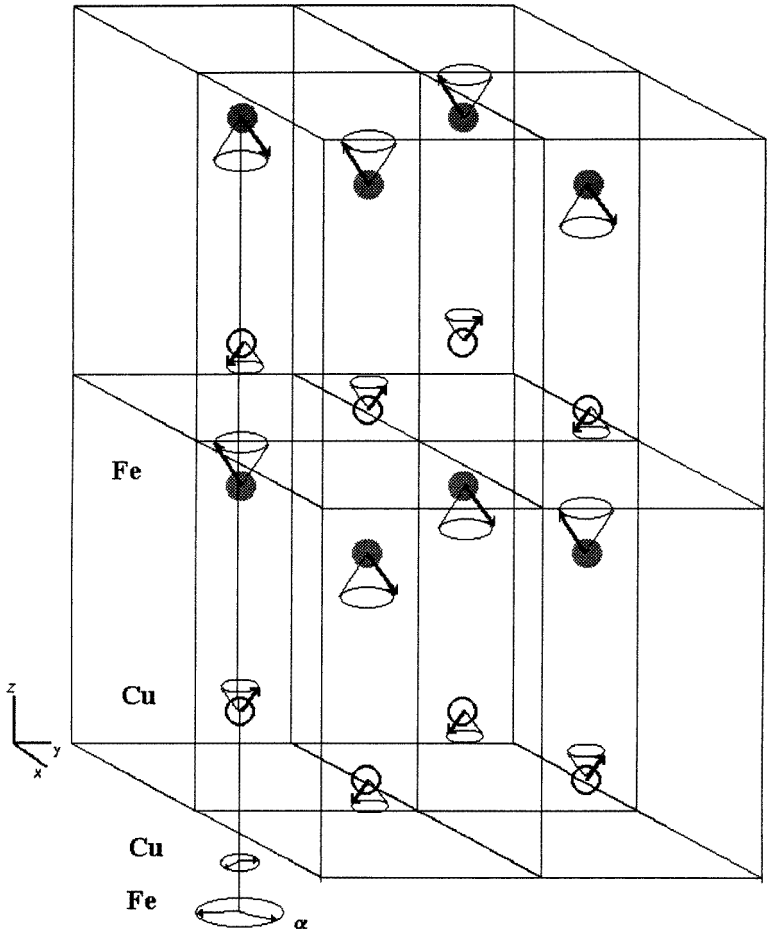

Figure 7. The proposed cone model. The figure shows the magnetic atoms (Fe^{3+} shaded spheres, Cu^{2+} open spheres) in the magnetic unit cell based on the expanded nuclear $P4mm$ model.

thus evident that the $P4/mmm$-based magnetic structure model is inferior to the $P4mm$-based one, failing to reproduce adequately peaks at lower-2θ regions. Careful inspection of the refined patterns in the low-2θ region (figure 2) shows that while it describes well the $(1/2, 1/2, 1/2)_M$ peak, it fails to reproduce the $(1/2, 1/2, 3/2)_M$ peak.

Taking into account these results, we then performed final nuclear and magnetic refinements of the high-resolution data over the 10°–150° 2θ range. In this case, we also explored the possibility of allowing anisotropic vibrations of the atoms in the unit cell. The Hamilton test for powder diffraction patterns [9] was used to determine whether any improvement in the R-factors was statistically significant. We thus found that for the fully ordered structure (space group $P4mm$) the atoms that show anisotropic motion are Y, Ba, Fe and the oxygen atoms corresponding to the iron square pyramid base; the copper ion and its environment (equatorial and apical oxygen atoms) retained isotropic thermal motion. For the fully disordered structure (space group $P4/mmm$), Y, Fe and Cu display isotropic motion, while barium and all oxygen atoms (both apical and equatorial) showed anisotropic

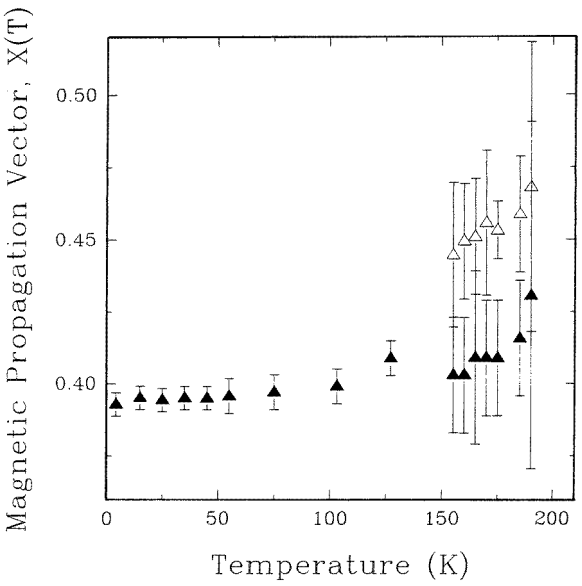

Figure 8. Evolution of the propagation vector of the incommensurate magnetic structures with temperature.

vibrational behaviour, in agreement with a previous report [7]. The final structural and magnetic Rietveld refinement in the region 10°–150° is shown in figure 3 for space group $P4mm$, while the parameters for both models are detailed in table 1 with selected bond lengths collected in table 2.

4. Structural and magnetic study in the temperature range 4.2–200 K

At temperatures below 190 K (figure 4), two new peaks appear straddling the most intense $(1/2, 1/2, 1/2)$ magnetic peak ($d \sim 5.15$ Å). The satellites are termed $(1/2, 1/2, 1/2)^+$ and $(1/2, 1/2, 1/2)^-$. No comparable satellites could be detected surrounding any of the other magnetic peaks of lower intensity. The magnetic nature of these peaks was confirmed by polarization analysis, as will be described in the next section. The intensities of the two $(1/2, 1/2, 1/2)^{\pm}$ peaks decrease with increasing temperature and disappear at ∼190 K. Careful inspection of the shape of the satellites (figure 4) further shows the existence of a splitting of the peaks in the temperature range 155–190 K. Figures 5 and 6 display the extracted temperature dependence of the positions and intensities, respectively, of the $(1/2, 1/2, 1/2)$ magnetic peak and its satellites.

At temperatures below 155 K, there is only one set of magnetic satellites. At 4.2 K, the $(1/2, 1/2, 1/2)^-$ peak is at 5.019(2) Å and the $(1/2, 1/2, 1/2)^+$ peak at 5.264(7) Å with normalized relative intensities of 0.40(6) and 0.16(4), respectively. In order to describe the low-temperature magnetic scattering results, the existence of a commensurate–incommensurate magnetic transition [10] at 190 K has to be invoked. The low-temperature incommensurate magnetic structure can be described as a helimagnetic structure with a magnetic propagation vector $\boldsymbol{k} = (1/2, 1/2, X(T))$ for which the satellites could be indexed as $(1/2, 1/2, 1/2)^+$ and $(1/2, 1/2, 1/2)^-$. This cone model is consistent with the perpendicular (μ_x, μ_y) components of the magnetic moment defining the spiral spin plane

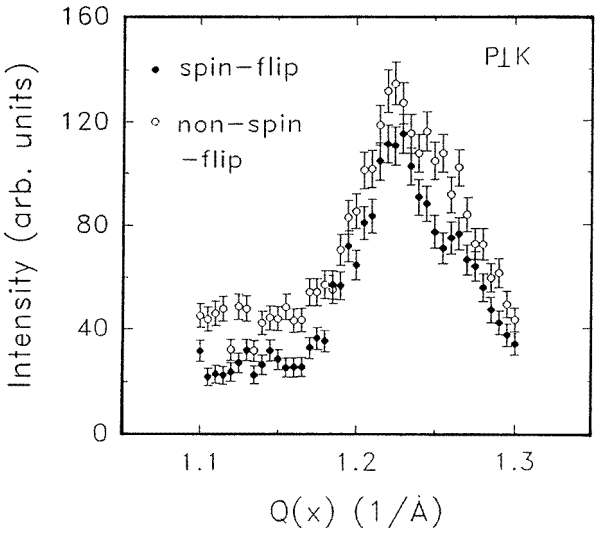

(a)

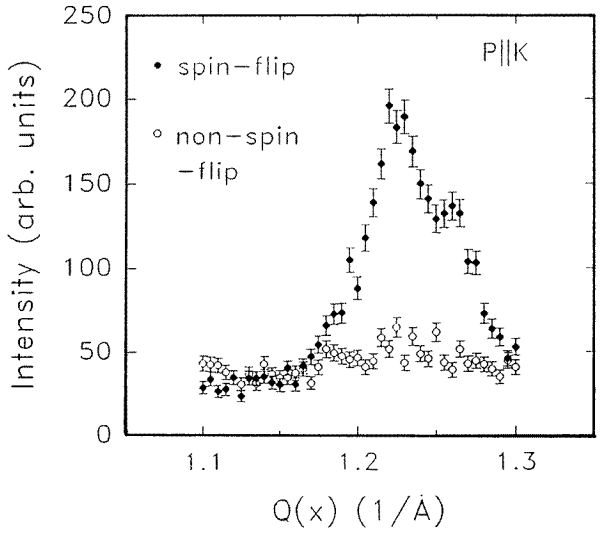

(b)

Figure 9. Polarization analysis in the $(1/2, 1/2, 1/2)_M$ peak region at 10 K. (a) Vertical field. (b) Horizontal field.

and the parallel component (μ_z) of the magnetic moment defining the fundamental single spin axis (figure 7). The angle of the helix can be then calculated as: $\alpha(T) = 2\pi \boldsymbol{k} \cdot \boldsymbol{c} = 2\pi(1/2, 1/2, X(T))\boldsymbol{c} = 2\pi X(T)$ and it displays a strong temperature dependence.

The existence of two sets of satellites, clearly visible in the 155–190 K temperature range, implies the presence of two incommensurate structures. The behaviour of the system is different below 155 K, as the two sets of symmetrically-displaced satellites about the central magnetic peak have collapsed to single peaks and a single incommensurate magnetic structure is evident. The magnetic propagation vectors for the incommensurate structures

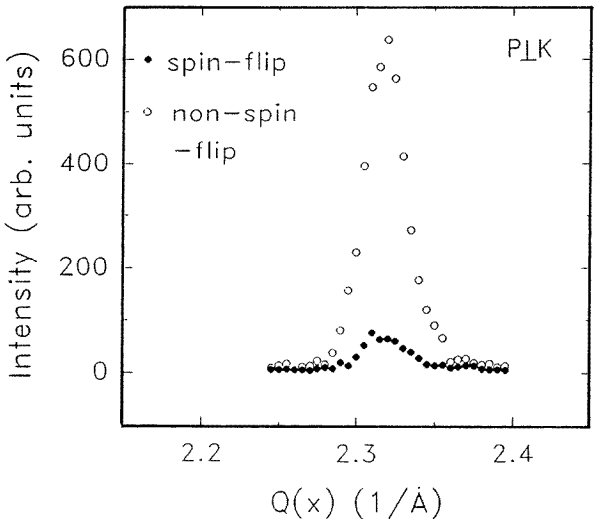

(a)

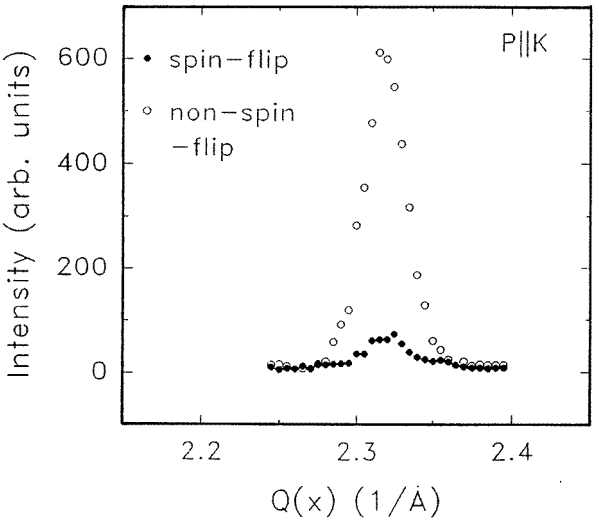

(b)

Figure 10. Polarization analysis in the $(102)_N$ and $(110)_N$ nuclear peak region at 10 K. (a) Vertical field. (b) Horizontal field.

below 180 K are shown as a function of temperature in figure 8 with X approaching a value of 0.393(5) at 4.2 K. The angles, α, of the magnetic helices can be also calculated using the earlier expression and are found to approach at 4.2 K a value of 141(2)°.

5. Polarization analysis

In order to verify the magnetic origin of the satellite peaks observed in $YBaCuFeO_{5+\delta}$ in the temperature range 4.2–190 K, we performed a series of measurements using polarized neutrons [11, 12]. The principle of this technique is based on the fact that when an applied

magnetic field $\boldsymbol{B}$ is parallel to the scattering vector $\boldsymbol{K}$, all scattering of magnetic origin is associated with a reversal of the neutron spin (spin-flip scattering). When $\boldsymbol{B} \perp \boldsymbol{K}$, both the spin-flip and non-spin-flip scattering are equally probable. Nuclear scattering, on the other hand, is independent of the relative orientation of $\boldsymbol{B}$ and $\boldsymbol{K}$.

Figure 9 displays the results obtained at 10 K in the $\boldsymbol{Q}$-region corresponding to the $(1/2, 1/2, 1/2)_M$ peak and its satellites. When the polarization vector is perpendicular to the scattering vector, there are approximately equal contributions to the scattering by spin-flip and non-spin-flip components (figure 9(a)), so that the final polarization is zero. However, when the initial polarization is along the scattering vector, only spin-flip scattering is observed (figure 9(b)). These results prove unambiguously the magnetic origin of the $(1/2, 1/2, 1/2)^{\pm}$ satellites, observed below $T = 190$ K. For comparison, we show in figure 10 the corresponding results of the measurements in the vicinity of the (102) and (110) nuclear peaks, whence only non-spin-flip scattering is observed irrespective of the relative orientation of the initial polarization and the scattering vector.

6. Conclusion

In conclusion, we have shown that the oxygen-deficient perovskite $YBaCuFeO_{5+\delta}$ phase exhibits a complicated magnetic behaviour with the appearance of an incommensurate magnetic structure below 190 K, characterized by two magnetic propagation vectors in the temperature range 155–190 K and a single magnetic propagation vector below 150 K. Rietveld refinements of high resolution diffraction data (taking into account both nuclear and magnetic scattering) favour a structure in which the Cu^{2+} and Fe^{3+} ions are fully ordered.

Acknowledgments

We thank the EPSRC, the British Council, the CONICYT and PEDECIBA (Uruguay) for financial support of this work and the National Institute of Standards and Technology, Gaithersburg, MD, USA and the Rutherford Appleton Laboratory, UK for provision of neutron time. We also thank A Lappas, M Adams and C Carlile for help with the experiments on IRIS.

References

[1] Er-Rakho L, Michel C, Lacorre P and Raveau B 1988 *J. Solid State Chem.* **73** 531
[2] Meyer C, Hartmann-Boutron F, Gros Y and Strobel P 1990 *Solid State Commun.* **76** 163
[3] Pissas M, Mitros C, Kallias G, Psycharis V, Niarchos D, Simopoulos A, Kostikas A, Christides C and Prassides K 1991 *Physica* C **185** 553
[4] Atanassova Y K, Popov V N, Bogachev G G, Iliev M N, Mitros C, Psycharis V and Pissas M 1993 *Phys. Rev.* B **47** 15 201
[5] Vaughey J T and Poeppelmeier K R 1991 *Proc. Int. Electronic Ceramics Conf. (1991) National Institute of Standards and Technology Special Publication* 804 p 419
[6] Mombrú A W, Christides C, Lappas A, Prassides K, Pissas M, Mitros C and Niarchos D 1994 *Inorg. Chem.* **33** 1255
[7] Caignaert V, Mirebeau I, Bourée F, Nguyen N, Ducouret A, Greneche J M and Raveau B 1995 *J. Solid State Chem.* **114** 24
[8] Larson A C and Von Dreele R B 1987 *Los Alamos National Laboratory Report* LA-UR-86-748
[9] Hamilton W C 1965 *Acta Crystallogr.* **18** 502
[10] Vigneron F 1986 *Chem. Scr.* A **26** 93
[11] Li W H, Lynn J W and Fisk Z 1990 *Phys. Rev.* B **41** 4098
[12] Moon R M, Riste T and Koehler W C 1969 *Phys. Rev.* B **181** 920